Optical absorption and single-particle excitations in the two-dimensional Holstein *t-J* model

B. Bäuml, G. Wellein, and H. Fehske
Physikalisches Institut, Universität Bayreuth, D-95440 Bayreuth, Germany
(Received 17 February 1998; revised manuscript received 16 April 1998)

To discuss the interplay of electronic and lattice degrees of freedom in systems with strong Coulomb correlations we have performed an extensive numerical study of the two-dimensional Holstein *t-J* model. The model describes the interaction of holes, doped in a quantum antiferromagnet, with a dispersionsless optical phonon mode. We apply finite-lattice Lanczos diagonalization, combined with a well-controlled phonon Hilbert space truncation, to the Hamiltonian. The focus is on the dynamical properties. In particular we have evaluated the single-particle spectral function and the optical conductivity for characteristic hole-phonon couplings, spin exchange interactions, and phonon frequencies. The results are used to analyze the formation of lattice hole polarons in great detail. Links with experiments on layered perovskites are made. In addition, we compare the Chebyshev recursion and maximum entropy algorithms, used for calculating spectral functions, with standard Lanczos methods. [S0163-1829(98)07428-1]

I. INTRODUCTION

There has been renewed interest in the analysis of strongly coupled electron-phonon (EP) systems since it was recognized that intrinsic polaronlike lattice distortions are a common feature of several important classes of perovskites such as the high-T_c cuprates,[1,2] the nonmetallic nickelates,[3] and the colossal magnetoresistance manganites.[4,5] In these compounds, e.g., in $La_{2-x}Sr_x[\,Cu/Ni\,]O_4$ or $La_{1-x}Ca_xMnO_3$, the charge carriers susceptible to lattice polaron formation mediate the antiferromagnetic (AFM) or ferromagnetic (FM) interactions between the Cu^{2+}, Ni^{2+} ($S=1/2,\ 1$), or Mn^{3+} ($S=3/2$) ions (core spins), suggesting that the local lattice or Jahn-Teller distortions play also a significant role in determining the electronic and magnetic properties.[6,7]

A number of experimental observations indicate spatial modulations of the spin and charge density in the copper-, nickel-, and manganese-based perovskites. For example, dynamical stripe correlations of spins and holes were found from neutron scattering[8] and x-ray absorption[9] (EXFAS) in superconducting $La_{1.85}Sr_{0.15}CuO_4$ and $YBa_2Cu_3O_{6.6}$. Rather static polaronic superlattice structures have been detected by electron,[10] neutron,[11] and x-ray diffraction[12] measurements in hole-doped (insulating) $La_{2-x}Sr_xNiO_4$. Local structure studies of $La_{1-x}Sr_xMnO_3$, performed using pulsed neutron powder diffraction and atomic pair-density function analysis,[13] suggest that nonuniform charge distributions related to lattice polarons exist in the paramagnetic, AFM, and FM phases, and are even present in the metallic state up to $x\sim 0.35$.

A striking feature of all these charge and spin ordering phenomena is their cooperative nature, demonstrating the strong interaction between spin, charge, and lattice degrees of freedom.[6,14] Accordingly, the lattice anomalies are well reflected in the transport properties. For example, there is observed a striking suppression of superconductivity in the $[La,Sr]_2CuO_4$ family compounds with $\sim 1/8$ doping, which is believed to have a connection with charge and spin stripe formation.[6] Undoubtedly, structural correlations and (polaronic) charge order are shown to be the driving force behind the pronounced resistivity anomalies found in $[La,Sr]_2NiO_4$ for hole concentrations 1/3 and 1/2.[10,15]

Since polaronic effects might be responsible for some of the puzzling thermodynamic and transport properties of the cuprates, nickelates, and manganites, increasing effort has been aimed to test the polaronic nature of charge carriers by means of optical experiments. One of the physical quantities that contains valuable information about the low-energy excitations in interacting EP systems is the optical conductivity, $\sigma(\omega)$, usually determined from reflectivity measurements. Here the anomalous broad optical absorption detected for the $La_{2-x}Sr_x[Cu,Ni]O_4$ compounds in several (normal-state) infrared experiments has attracted a lot of attention. In particular for the nickelate system, where the existence of self-trapped charge carriers is well established, the midinfrared absorption band has been interpreted successfully in terms of photon-assisted hopping of small-size lattice polarons.[16,17] On the other hand, from a comparison of the optical absorption of several perovskites ($La_{1.67}Sr_{0.33}NiO_4$, $Sr_{1.5}La_{0.5}MnO_4$, and $Nd_{1.96}Ce_{0.04}CuO_4$), it has been argued that in the low-doping cuprates the lattice polarons appear to be rather large.[18,19] Although recent time-resolved optical relaxation measurements on $YBaCuO_{7-\delta}$ give additional evidence for the existence of polaronic carriers in the cuprates,[20] it is worth mentioning that the present experimental situation certainly does not permit one to draw any decisive conclusion concerning the relevance of the polaron/bipolaron scenario for high-T_c superconductivity.

From a theoretical point of view, the main problem for a proper treatment of such systems, exhibiting besides a substantial EP coupling strong Coulomb correlations, is that the coherent motion of charge carriers, heavily dressed, e.g., by interaction with magnons, takes place on a strongly reduced energy scale being almost comparable to the relevant phonon frequencies. As a result the standard strong-coupling Migdal-Eliashberg approach based on the adiabatic Migdal theorem might break down,[21,22] and it has been argued that nonadiabatic vertex corrections are responsible for the enhancement of T_c.[23–25] Furthermore, as a consequence of the preexisting

 © 1998 The American Physical Society

magnetic ''self-localization'' of the charge carriers, polaronic effects play an important role even at rather moderate EP coupling strengths.[26–30] Therefore the investigation of such highly correlated EP systems is of fundamental importance, not only in connection with the high-T_c problem.

Our aim here is to study what is perhaps the minimal microscopic model with respect to a strong spin-charge-lattice coupling, the so-called Holstein t-J model (HtJM). The focus is on the spectral properties of the HtJM Hamiltonian in the single-hole subspace relevant to the physically most interesting low doping regime. In order to obtain reliable results for the complete range of exchange interactions, EP couplings, and phonon frequencies we will employ numerical exact diagonalization (ED) techniques on finite lattices, using massive parallel computers such as the CRAY T3E.

The paper is organized as follows: In the next section we introduce the HtJM and comment on previous numerical investigations. Section III presents our ED results for the single-particle spectral function, which will be used in Sec. IV to discuss the hole-polaron band formation. In Sec. V we analyze the optical response in the HtJM. Our main results are summarized in Sec. VI. A comparative study of several computational techniques proposed for calculating spectral properties of very large Hamiltonian matrices is performed in the Appendix.

II. THE HOLSTEIN t-J MODEL

Our model is the standard two-dimensional t-J model appended by an additional Holstein-like interaction term with a dispersionless (optical) phonon branch:

$$\mathcal{H}=-t\sum_{\langle ij\rangle\sigma}(\tilde{c}^{\dagger}_{i\sigma}\tilde{c}_{j\sigma}+\text{H.c.})+J\sum_{\langle ij\rangle}(\vec{S}_i\vec{S}_j-\tfrac{1}{4}\tilde{n}_i\tilde{n}_j)$$
$$-\sqrt{\varepsilon_p\hbar\omega_0}\sum_i(b^{\dagger}_i+b_i)\tilde{h}_i+\hbar\omega_0\sum_i(b^{\dagger}_i b_i+\tfrac{1}{2}). \quad (1)$$

The Holstein t-J Hamiltonian (1) acts in a projected Hilbert space without doubly occupied sites, where $\tilde{c}^{(\dagger)}_{i\sigma}=c^{(\dagger)}_{i\sigma}(1-\tilde{n}_{i,-\sigma})$ is a spin-σ electron annihilation (creation) operator on Wannier site i, $\tilde{n}_i=\Sigma_\sigma\tilde{c}^{\dagger}_{i\sigma}\tilde{c}_{i\sigma}$, and $\vec{S}_i=\Sigma_{\sigma,\sigma'}\tilde{c}^{\dagger}_{i\sigma}\vec{\tau}_{\sigma\sigma'}\tilde{c}_{i\sigma'}$. Within an effective single-band description, the parameters t and J measure the transfer amplitude and the antiferromagnetic exchange interaction between nearest-neighbor sites on a square lattice, where $t>J$ corresponds to the situation in the cuprates. For example, $J/t\simeq 0.4$ with $t\simeq 0.3$ eV is commonly used to model the $La_{2-x}Sr_xCuO_4$ system. In Eq. (1), we have chosen the coupling to the hole, $\tilde{h}_i=1-\tilde{n}_i$ is the local density operator of the spinless hole, as the dominant source of the EP coupling, because in the t-J model the unoccupied site corresponds to the Zhang-Rice singlet (formed from Cu $3d_{x^2-y^2}$ and O $2p_{x,y}$ hole orbits) for which the coupling should be much stronger than for the occupied (Cu^{2+}) site.[31–33] The hole-phonon coupling constant is denoted by ε_p, and $\hbar\omega_0$ is the bare phonon frequency (below $\hbar=1$ and all energies are measured in units of t). Then $q_i=(b^{\dagger}_i+b_i)/\sqrt{2M\omega_0}$ may be thought of representing an internal vibrational degree of freedom of the lattice site i [$b^{(\dagger)}_i$ annihilates (creates) an optical phonon]. Indeed for $La_2[Cu,Ni]O_4$ the oxygen vibrational modes have a small dispersion in the Brillouin zone, i.e., they are revealed to be very localized in real space and can be considered as independent.[34]

Whereas the electronic properties of the pure t-J model have been studied extensively in the context of high-T_c superconductivity,[35] very little is known theoretically about the interplay between magnetic exchange interaction and EP coupling in the framework of the 2D HtJM. The changes of the quasiparticle (QP) properties due to the cooperative/competitive effects of the hole-phonon and hole-magnon interactions are expected to be very complex and as yet there exist no well-controlled analytical techniques to solve the problem particularly in the physically relevant coupling regime, where the characteristic electronic (t,J) and phononic (ε_p,ω_0) energy scales are not well separated. Naturally such a dressed hole QP will show the characteristics of both ''lattice'' and ''magnetic'' (hole) polarons.[36]

Early attempts to study lattice polaron effects in the HtJM were based on a variational squeezed-polaron approach to the phonon subsystem.[30] The effective electronic Hamiltonian, obtained in the transformed phonon vacuum state, was treated by means of Gutzwiller or slave boson techniques and the main features of the ground-state phase diagram of the Holstein Hubbard/t-J models were worked out on a mean-field level of approximation.[37,38] Analyzing the static charge susceptibility of the HtJM, a transition to a Peierls distorted phase was found to occur at quarter filling.[39] In the low-doping regime and for moderate EP interactions the lowest polaron-magnon band states were determined for the Lang-Firsov transformed 2D HtJM within the zero-phonon and spin-wave approximations, indicating the formation of large size (mainly magnetic) hole polarons with solitonlike-shaped highly asymmetric wave functions, oriented along the diagonals of the square lattice.[40] Combining the spin-wave approximation with an iterative Lanczos algorithm, the ground-state properties of the 2D HtJM were examined including multiphonon states.[41] A sharp crossover to small size less dispersive symmetric lattice hole polarons was obtained at a critical value of the EP coupling.[41] Using the self-consistent Born approximation, the phonon-induced mass renormalization of a hole in the HtJM was found to depend strongly on the confining string potential due to the spin background.[21] Whereas a large AFM exchange interaction certainly enhances the tendency towards lattice polaron formation, there is evidence that in the limit $J\to 0$ the influence of phonons becomes even smaller than in the corresponding uncorrelated (spinless fermion) model.[21] More recently, the single-hole spectral density function and the optical conductivity were studied within the noncrossing approximation for spin-wave and phonon interactions in a Holstein t-J–like Hamiltonian.[22] Perhaps surprisingly, the numerical estimate of the lowest-order vertex corrections to the hole-phonon coupling vertex gives relatively small values, indicating that Migdal's approximation can be used in calculating the hole self-energy. This effect has been attributed to the significant suppression of the QP residue for a correlated electron system.[22]

Of course these analytical approaches provide some insight into the problem, but it is difficult to judge how close to

the actual properties of the HtJM the results are. From this point of view it is of interest to carry out exact diagonalizations of the HtJM on small clusters. Along this line, a number of ED studies have been performed treating the phonons in the static limit, i.e., classically, in the so-called adiabatic or frozen-phonon approximation.[42,31,43,44] The stability of the ground state against static lattice distortions was investigated and the phase diagram of the 2D HtJM has been explored in the one- and two-hole sectors,[31] as well as for the quarter-filled band case,[44] where a polaronic superlattice was found to occur above a critical EP coupling strength. Neglecting, however, the phonon dynamics certainly overestimates the tendency towards lattice polaron or charge-density-wave (CDW) formation.[45,46] As a first step to overcome the static treatment of the HtJM, a variational Lanczos diagonalization technique has been proposed,[26] which is based on an inhomogeneous modified Lang-Firsov transformation and allows for the description of static displacement field, nonadiabatic lattice polaron and squeezing effects on fairly large clusters. Extending the ED approach to the full quantum phonon model requires a truncation of the bosonic part of the Hilbert space, which, strictly speaking, is infinite dimensional. Including at each site besides the phonon vacuum a second (coherent) displaced oscillator state, the 1D HtJM has been analyzed with respect to the occurrence of CDW order, superconducting fluctuations, and phase separation.[45] Whether the complex (phonon-assisted) transport in the HtJM can be described with sufficient accuracy within such a simple two-state variational approach remains questionable, at least in the intermediate coupling regime. For the 2D case more advanced truncation procedures in momentum space, retaining a single or small number of phonon modes,[34,47] have been employed to show that dynamical in-plane phonons could help to stabilize inhomogeneous stripelike phases. Taking into account all dynamical phonon modes, in a previous work[27] the authors have examined the ground-state properties of the 2D Holstein t-J model in the one- and two-hole subspaces by means of direct Lanczos diagonalization. Most notably, the transition from delocalized to self-trapped lattice hole polarons (hole bipolarons), signaled by a suppression of the kinetic energy and an enhancement of the hole-phonon (hole-hole) correlation functions, was found to be favored by strong Coulomb correlations.

In the present paper, we extend this rigorous approach, which preserves the full dynamics and quantum nature of phonons, to the calculation of dynamical quantities. In particular we compute the single-hole spectral function and the optical conductivity to discuss the transport of hole polarons in the framework of the 2D HtJM. The technical details of the computational procedures such as the basis implementation and symmetrization, the phonon Hilbert space truncation and the spectral moment approach will be discussed in the Appendix.

III. SINGLE-PARTICLE SPECTRAL PROPERTIES

In the numerical analysis of the 2D HtJM we start with a discussion of the single-hole spectral function

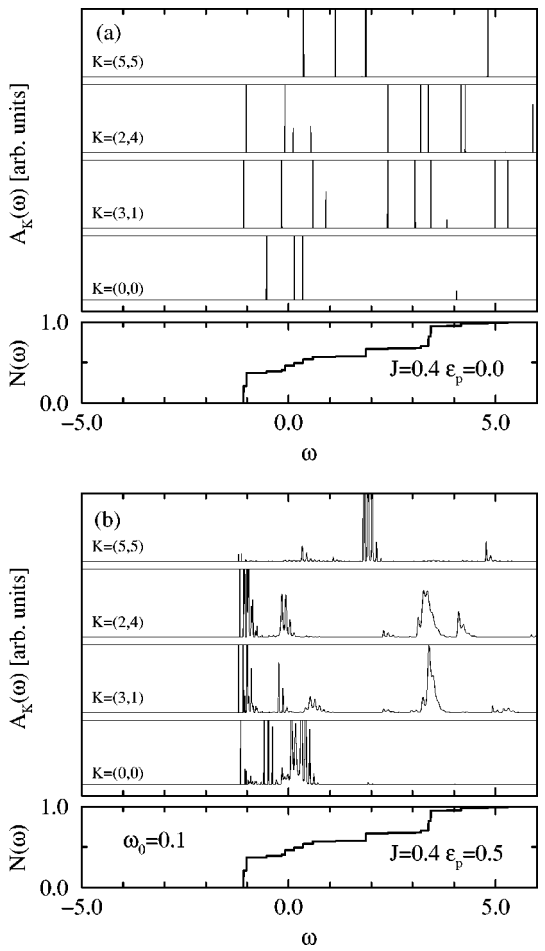

FIG. 1. Wave-vector resolved spectral functions of one hole in the t-J (a) and Holstein t-J (b) models. Results are obtained for a tilted $\sqrt{10}\times\sqrt{10}$ cluster with periodic boundary conditions [$\vec{K}$ vectors are given in units of $(\pi/5,\pi/5)$]. The integrated densities of states are depicted in the lower panels of (a) and (b). The units of $A_{\vec{K}}$, though arbitrary, are nevertheless the same in all $\vec{K}$ sectors displayed in Figs. 1–3, so that the peak heights may be compared.

$$A_{\vec{K}}(\omega)=\sum_{n,\sigma}|\langle\Psi_{n,\vec{K}}^{(N-1)}|\tilde{c}_{\vec{Q}-\vec{K},\sigma}|\Psi_{0,\vec{Q}}^{(N)}\rangle|^2 \times\delta[\omega-(E_{n,\vec{K}}^{(N-1)}-E_{0,\vec{Q}}^{(N)})]. \quad (2)$$

Figure 1 displays $A_{\vec{K}}(\omega)$ for the allowed values of the momentum $\vec{K}$ of a ten-site square lattice. To visualize the intensities (spectral weights) connected with the various peaks (excitations) in each $\vec{K}$ sector we also have shown the integrated density of states

$$N(\omega)=\int_{-\infty}^{\omega}d\omega'\frac{1}{N}\sum_{\vec{K}}A_{\vec{K}}(\omega'). \quad (3)$$

Of course, in the absence of EP coupling we reproduce the single-particle spectrum of the pure t-J model, which for comparison is shown in Fig. 1(a). In this case the single-hole excitations are reasonably well understood.[35] $A_{\vec{K}}(\omega)$ contains a ''quasiparticle'' peak at the bottom of the spectrum followed by a lump of spectral weight with some internal structure. The QP pole, corresponding directly to the coher-

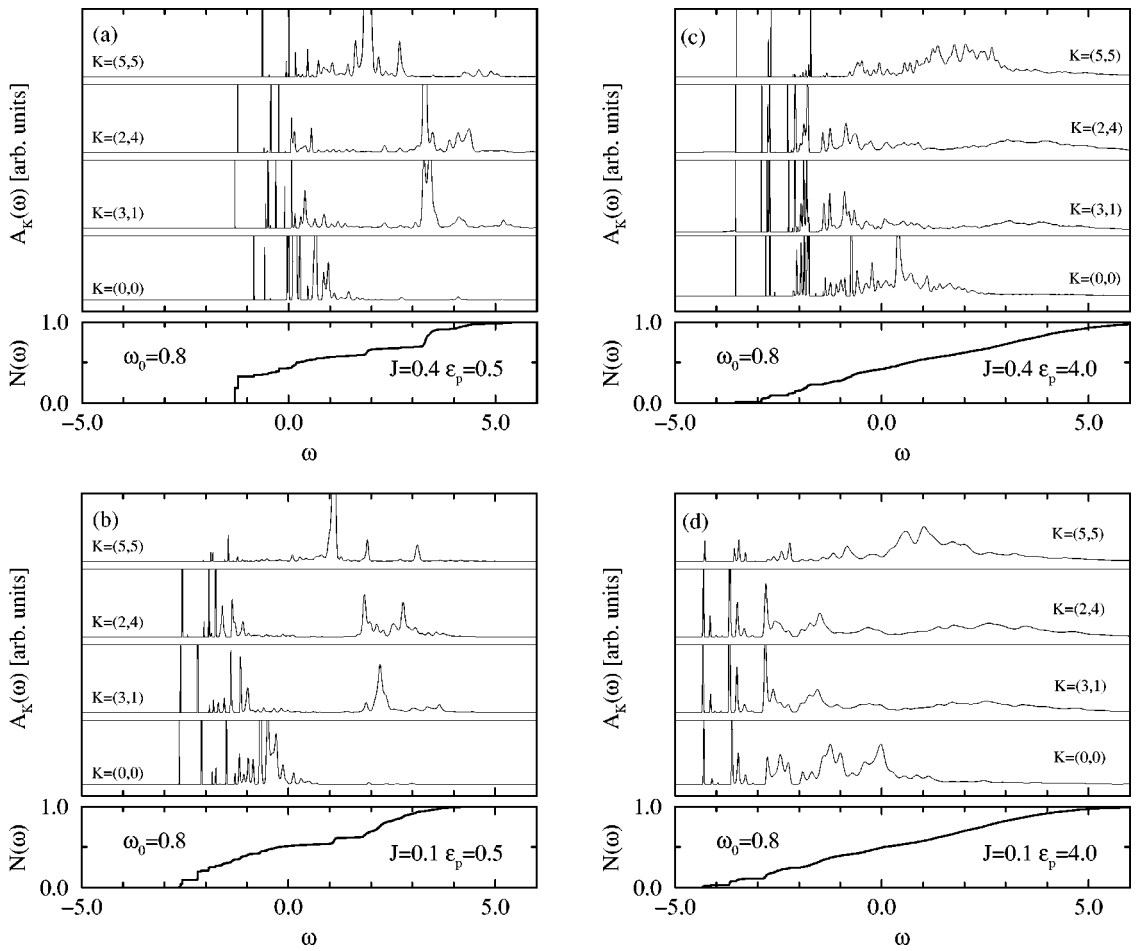

FIG. 2. Single-hole spectral function $A_{\vec{K}}(\omega)$ and integrated spectral weight $N(\omega)$ for the 2D HtJM at $\omega_0=0.8$ for different values of ε_p and J. Note that the lowest peak in (c) and (d) contains contributions from each $\vec{K}$ sector.

ent single-hole ground state with momentum $(3\pi/5,\pi/5)$ is separated by a pseudogap of approximative size J from the lower edge of a broad incoherent continuum $6t$ wide. Despite the significant redistribution of intensity to higher energies as a consequence of multiple spin-wave (spinon) scattering of the magnetic polaron,[48] the QP residue still contains a substantial amount of spectral weight. It has been argued that the QP peak and the low-energy satellite structures, which can be identified as the next excited states of the string problem, will survive in the bulk limit.[35] The momentum dependences of $A_{\vec{K}}(\omega)$ indicate that the low-energy structure of the $\vec{K}$-integrated spectrum is dominated by excitations with wave vectors near the magnetic Brillouin zone boundary [particularly by the $\vec{K}$ vectors closest to $(\pi/2,\pi/2)$ and $(\pi,0)$].[49] On the other hand, for momenta $\vec{K}=(0,0)$ and (π,π) most of the weight of $A_{\vec{K}}$ is concentrated at high energies, i.e., in the incoherent part of the spectrum.

Now we consider the influence of an additional weak EP interaction [Fig. 1(b)]. In the weak-coupling regime the mass renormalization of the coherent QP band due to the hole-phonon coupling is generally small compared with that arising from the hole-spin interactions (magnetic polaron regime). In particular, the integrated densities of states are barely changed from those of the pure t-J model. The new structures, nevertheless observed in the $A_{\vec{K}}$ spectra shown in Fig. 1(b), correspond to predominantly ''phononic'' side bands separated from the particle-spin excitations by multiples of the bare phonon frequency ω_0. However, these phonon resonances have less and less ''electronic'' spectral weight the more phonons are involved. This is because $A_{\vec{K}}(\omega)$ measures the overlap of these excited states with the state obtained by creating a hole in the *zero-phonon* Heisenberg ground state.

To analyze the formation of lattice hole polarons in the 2D HtJM, we have compared the nonadiabatic weak- and strong-coupling situations in Fig. 2. Looking first at the case $J=0.4$, panels (a) and (c), we observe that with increasing ε_p the lowest peaks in each $A_{\vec{K}}$ start to separate from the rest of the spectrum. These states become very close in energy and finally a narrow well-separated lattice hole-polaron band evolves in the strong-coupling case ($\varepsilon_p=4.0$). Since the gap to the next energy ''band'' is of the order of ω_0 [see panel (c)], these excitations will be triggered by an one-phonon absorption process. The transition to the lattice hole-polaron state is accompanied by a strong increase in the on-site hole-phonon correlations,[27] indicating that the lattice polaron QP comprising a ''quasilocalized'' hole and the phonon cloud is mainly confined to a single lattice site (small size lattice hole polaron). Compared to the noninteracting single-electron (Holstein model) (Ref. 50) or spinless fermion (Holstein-t model) (Ref. 26) problems, the critical EP coupling strength for lattice polaron formation is considerably reduced due to

magnetic prelocalization effects. The phonon distribution function shows that the small size lattice hole-polaron state is basically a multiphonon state (see Ref. 51; cf. also Fig. 8 in the Appendix). For example, at $\varepsilon_p=4.0$ and $J=0.4$ we found the mean phonon number in the ground state to be about 4–5. Here the phonons will heavily dress the hole and the QP pole strength becomes strongly suppressed (cf. the discussion in Sec. IV). At the same time spectral weight is transferred to the high-energy part and the whole spectrum becomes incoherently broadened. Therefore, we observe an overall smoothing of $N(\omega)$. We note that the vertex corrections to the hole-phonon vertex are non-negligible for the large hole-phonon couplings and intermediate phonon frequencies considered here ($\varepsilon_p, \sqrt{\varepsilon_p\omega_0} \gtrsim J$). This has to be contrasted with the weak to moderate EP coupling regimes, where the vertex correction was found to be much smaller than unity.[22]

Next, we want to discuss the effect of the exchange interaction J. For the t-J model it is well known that as long as J/t is large, i.e., the spins are antiferromagnetically ordered, the delocalization of a hole is hindered as a consequence of a linear confining string potential originated from the misaligned spins along the hole hopping paths. If J tends to zero, the string potential is weakened and the hole performs large excursions polarizing the spin background ferromagnetically. In a finite system this so-called Nagaoka transition takes place at a *finite* critical exchange interaction ($J_N=0.138$ for the ten-site lattice). For $J<J_N$, the single-hole ground state has momentum $\vec{K}=(0,0)$ and is fully spin aligned. At $J=0$, the spectrum is completely incoherent, extending over almost the unperturbed bandwidth $8t$. As can be seen from Fig. 2(b), showing the case $J=0.1<J_N$, a weak EP coupling does not affect this scenario. Quite the reverse, from a self-consistent Born calculation it was deduced that the influence of phonons on such a ''Nagaoka spin-polaron'' becomes even smaller than in the free fermion case.[21] The situation, however, is changed completely in the strong EP coupling regime. As ε_p increases, the mobility of the hole is reduced and finally a strong local lattice distortion traps the hole almost on a single site. The hole-trapping makes even a small AFM exchange interaction very effective and we observe, as for the static ($\omega_0\to 0$) HtJM,[43] an enhancement of the AFM correlations in the spin background. Consequently, the whole spectrum looks very similar to that obtained for $J=0.4$ [cf. panels (c) and (d)]. The only difference is that now the first spin excitations, having an excitation energy $\propto J^{(2/3)}$,[52] occur just above the lattice hole-polaron band, thus filling the gap between the first and second polaronic bands.

Finally, we consider the regime where the bare phonon frequency is much larger than the effective hole bandwidth of the t-J model. For $0.1\leqslant J\leqslant 0.4$, the coherent bandwidth can be approximated by $\Delta E^{t-J}\simeq 1.5J^{\alpha}$ with $\alpha\simeq 1$.[53] Figure 3 shows the results for the spectral function $A_{\vec{K}}(\omega)$ at $\omega_0=3.0$, $\varepsilon_p=4.0$, and $J=0.4$. In this case the lowest (QP) excitation band is only weakly renormalized by the phonons that can follow the motion of the magnetic polaron instantaneously. The weights of the first m-phonon states in the ground state are 0.436, 0.332, 0.15, and 0.055 for $m=0$, 1, 2, and 3, respectively. As can be seen by comparing Figs. 1(a), 2(c), and 3, the QP pole strength is determined by the subtle interplay of ε_p and ω_0. In the antiadiabatic strong-coupling limit, the high-energy part of the $A_{\vec{K}}(\omega)$ spectrum is clearly dominated by interband transitions according to multiphonon absorptions [cf. the pronounced jumps in $N(\omega)$ at energies $\omega\simeq n\times\omega_0$].

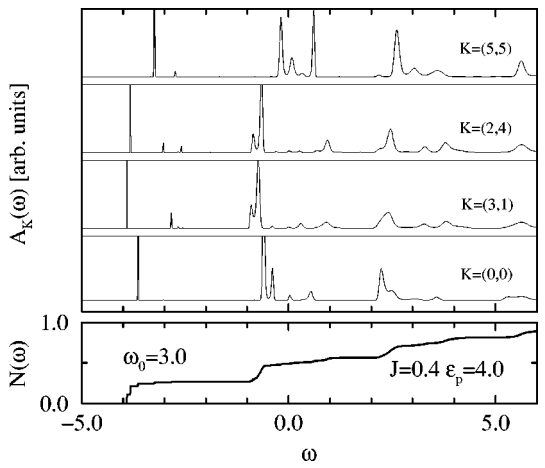

FIG. 3. $A_{\vec{K}}(\omega)$ and $N(\omega)$ for the 2D HtJM in the nonadiabatic strong EP coupling regime ($\omega_0=3.0$, $\varepsilon_p=4.0$).

IV. POLARON BAND FORMATION

To illustrate the formation of the lattice hole-polaron band in some more detail, we have calculated the ''coherent'' band dispersion of the 2D HtJM, $E_{\vec{K}}$, on a 16-site lattice. $E_{\vec{K}}$ was determined from the lowest pole of each $A_{\vec{K}}(\omega)$ having finite spectral weight. The resulting band structure is shown in Fig. 4 along the principal directions in the Brillouin zone. For the pure t-J model, the dispersion of the QP band is highly consistent with a simple tight-binding form[54] that includes hole hopping processes to first and second-nearest neighbors on the same sublattice only (leaving the magnetic order undistorted). From Fig. 4(a) the minima of the QP dispersion are found to be located at the momenta $\vec{K}=(\pm\pi/2,\pm\pi/2)$ [the hidden symmetry of the 4×4 cluster leads to an accidental degeneracy with the $\vec{K}=(\pm\pi,0)$, $(0,\pm\pi)$ states]. Obviously, the energy dispersion is not significantly changed including a weak EP coupling, provided that the phonon frequency exceeds the effective bandwidth of the magnetic polaron ($\omega_0=0.8\geqslant\Delta E^{t\text{-}J}$). On the other hand, in the adiabatic regime ($\omega_0\ll\Delta E^{t\text{-}J}$), a remarkable ''flattening'' of the band structure of the HtJM takes place, which can be attributed to the ''hybridization'' of the hole QP band with the dispersionless optical phonon. As a result the coherent bandwidth $\Delta E=\sup_{\vec{K}}E_{\vec{K}}-\inf_{\vec{K}}E_{\vec{K}}$ is roughly given by ω_0.

In order to make this discussion more quantitative, we have evaluated numerically the spectral weight of the different band states,

$$Z_{\vec{K}}=\frac{|\langle\Psi^{(N-1)}_{0,\vec{K}}|\tilde{c}_{\vec{Q}-\vec{K},\sigma}|\Psi^{(N)}_{0,\vec{Q}}\rangle|^2}{|\langle\Psi^{(N)}_{0,\vec{Q}}|\tilde{c}^{\dagger}_{\vec{Q}-\vec{K},\sigma}\tilde{c}_{\vec{Q}-\vec{K},\sigma}|\Psi^{(N)}_{0,\vec{Q}}\rangle|^2}, \tag{4}$$

where $|\Psi^{(N-1)}_{0,\vec{Q}}\rangle$ denotes the one-hole (polaron) state being lowest in energy within the $\vec{Q}$ sector. The results for $Z_{\vec{K}}$ are

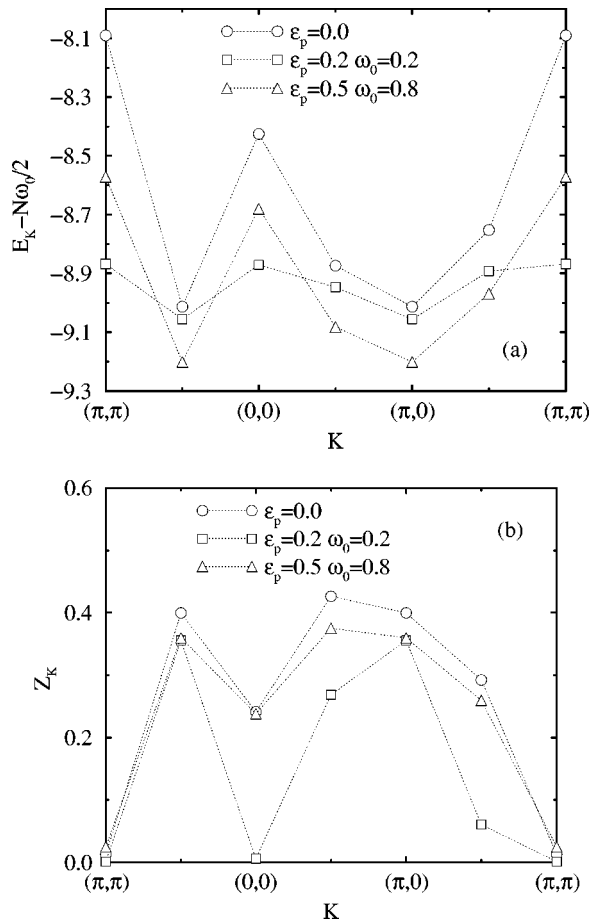

FIG. 4. Band dispersion (a) and spectral weight factors (b) for the 2D HtJM on a 16-site lattice ($J=0.4$).

displayed in Fig. 4(b). As already discussed in Sec. III, $Z_{\vec{K}}$ is strongly reduced from unity in the pure t-J model (but seems to remain finite in the thermodynamic limit if $J>0$). Including a weak adiabatic EP interaction ($\varepsilon_p=0.2$, $\omega_0=0.2$), the band states with energies larger than $E_0+\omega_0$ change their character from ''holelike'' to ''phononlike.'' Consequently, we observe a nearly complete suppression of $Z_{(0,0)}$ and $Z_{(\pi,\pi/2)}$. Increasing the phonon frequency, this tendency is reversed (see the curve for $\omega_0=0.8$). Note that similar effects have been discussed quite recently in terms of the single-electron Holstein model.[55,56]

To complete this section, we show in Fig. 5 the variation of $Z_{\vec{K}}$ with the EP coupling strength for the $\vec{K}$ vectors of the ten-site lattice studied in Sec. III. The wave-function renormalization factor $Z_{\vec{K}}$ can be taken as a measure of the ''contribution'' of the hole (dressed at $\varepsilon_p=0$ by spin-wave excitations) to the polaronic QP (having total momentum $\vec{K}$). The data obtained at weak EP coupling unambiguously confirm the different nature of band states in this regime: we found practically zero-phonon ''hole'' states at the band minima [$\vec{K}=(3\pi/5,\pi/5)$, triangles down] and ''phonon'' states, which are only weakly affected by the hole, around the (flat) band maxima [$\vec{K}=(\pi,\pi)$, triangles up]. With increasing ε_p, a strong ''mixing'' of holes and phonons takes place, whereby both quantum objects completely lose their own identity. Concomitantly $Z_{\vec{K}}$ decreases for the ''holelike'' states but increases (first of all) for the ''phononlike''

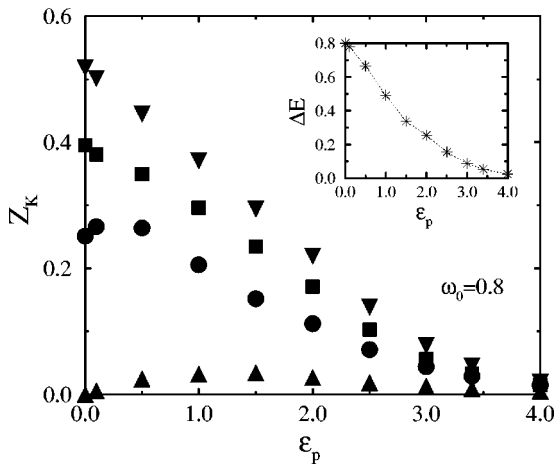

FIG. 5. Spectral weight factor $Z_{\vec{K}}$ as a function of the EP coupling strength ε_p for the different $\vec{K}$ vectors of the ten-site lattice: (3,1) (triangles down), (2,4) (squares), (0,0) (circles), and (5,5) (triangles up) [in units of $(\pi/5,\pi/5)$]. The inset shows the narrowing of the coherent bandwidth ΔE with increasing ε_p.

states. At large ε_p, a small lattice hole polaron is formed, which, according to the numerical results, has an extremely small spectral weight. Hence the question arises whether the lattice hole polaron is a ''good'' QP in the sense that one can construct a QP operator, $\tilde{c}_{\vec{K}\sigma}\rightarrow\tilde{d}_{\vec{K}\sigma}$, having large spectral weight at the lowest pole in the spectrum. Indeed, it was demonstrated in recent ED work that it is possible to construct such a composite electron/hole-phonon (polaron) operator by an appropriate phonon dressing of $\tilde{c}_{\vec{K}\sigma}$ for the Holstein model[50] as well as for the t-J model coupled to buckling/breathing modes.[29]

V. OPTICAL CONDUCTIVITY

Using standard linear response theory, the Kubo formula for the real (absorbent) part of the frequency-dependent optical conductivity gives two physically distinct contributions:[57,58]

$$\mathrm{Re}\ \sigma_{xx}(\omega)=\mathcal{D}\delta(\omega)+\sigma_{xx}^{reg}(\omega),\quad \omega\geq 0. \tag{5}$$

The first so-called Drude term at $\omega=0$ is due to the free acceleration of the charge carriers by the electric field and the second term, frequently called the ''regular term,'' is due to finite frequency dissipative optical transitions to excited quasiparticle states. More explicitly, the regular part can be written in spectral representation at $T=0$ as[35]

$$\sigma_{xx}^{\mathrm{reg}}(\omega)=\frac{e^2\pi}{N}\sum_{n\neq 0}\frac{|\langle\Psi_{n,\vec{K}}^{(N-1)}|\hat{j}_x^{(p)}|\Psi_{0,\vec{K}}^{(N-1)}\rangle|^2}{E_{n,\vec{K}}^{(N-1)}-E_{0,\vec{K}}^{(N-1)}}\times\delta[\omega-(E_{n,\vec{K}}^{(N-1)}-E_{0,\vec{K}}^{(N-1)})], \tag{6}$$

where the summation is taken over the complete set of eigenstates with excitation energies $\omega=[E_{n,\vec{K}}^{(N-1)}-E_{0,\vec{K}}^{(N-1)}]$ in the one-hole ($N-1$ electron) subspace. For the HtJM the (paramagnetic) current density operator $j_x^{(p)}$ has the form

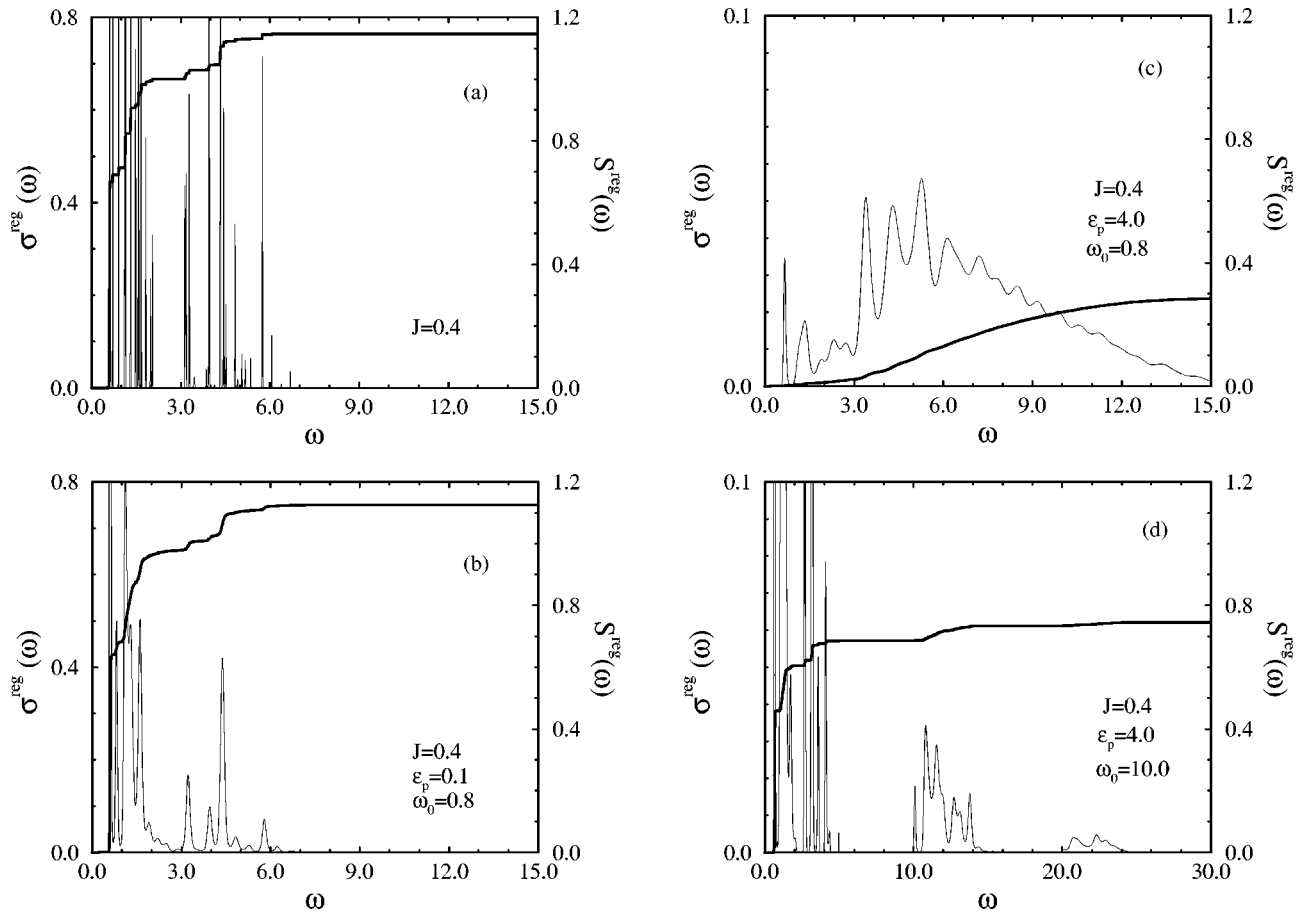

FIG. 6. Optical conductivity in the 2D (Holstein) t-J model for $J=0.4$. $\sigma^{\mathrm{reg}}(\omega)$ and $S^{\mathrm{reg}}(\omega)$ are obtained for the ten-site lattice with 15 phonons. The single-hole ground state has momentum $\vec{K}=(3\pi/5,\pi/5)$.

$$j_x^{(p)}=it\sum_{i\sigma}\,(\tilde{c}_{i,\sigma}^{\dagger}\tilde{c}_{i+x,\sigma}-\tilde{c}_{i+x,\sigma}^{\dagger}\tilde{c}_{i,\sigma}). \tag{7}$$

Actually in Eq. (6) an optical transition can take place only within the $\vec{K}$ sector of the ground state.

The expression (6) has been used to calculate $\sigma^{\mathrm{reg}}(\omega)$ numerically for the t-J (e.g., see Ref. 35) and Holstein models[59,60,50] on finite lattices employing ED techniques. First results, obtained recently for the 1D HtJM,[32] indicate that EP coupling effects may be at least partly responsible for the experimentally observed frequency dependence of the optical conductivity in the CuO_3 chains of the 1:2:3 family of high-T_c oxides.

In Fig. 6 we show $\sigma^{\mathrm{reg}}(\omega)$ of the 2D ten-site HtJM, determined from Eq. (6) with at most $M=15$ phonons, for typical values of the hole-phonon coupling and $J=0.4$. In the weak EP coupling regime and for phonon frequencies $\omega_0 \gtrsim \Delta E^{t\text{-}J}$, we recover the main features of the optical absorption spectrum of the 2D t-J model,[61] i.e., an ''anomalous'' broad midinfrared band [$J\lesssim\omega\lesssim 2t$], separated from the Drude peak [$\mathcal{D}\delta(\omega)$; not shown] by a ''pseudogap'' $\simeq J$, and an ''incoherent'' tail up to $\omega\simeq 7t$ [compare panels (a) and (b)]. Note particularly the even quantitative agreement between the ω-integrated spectral weight functions

$$S^{\mathrm{reg}}(\omega)=\int_0^{\omega} d\omega'\,\sigma_{xx}^{\mathrm{reg}}(\omega') \tag{8}$$

depicted in Figs. 6(a) and 6(b). Since for the parameters used in Fig. 6(b), $\varepsilon_p=0.1$ and $\omega_0=0.8$, the averaged kinetic energy per site $\langle -\mathcal{H}_t/N\rangle$ is only weakly renormalized by the EP interaction [cf. Fig. 10 of Ref. 27; $\mathcal{H}_t$ denotes the first term in (1)], also the Drude weight

$$\mathcal{D}=\frac{\pi e^2}{2N}\langle -\mathcal{H}_t\rangle - 2S^{\mathrm{reg}}(\infty), \tag{9}$$

obtained via the f-sum rule, should approximately be the same as for the noninteracting system ($\varepsilon_p=0$). As discussed in the preceding section, the coherent band structure gets stronger renormalized at large ε_p, i.e., the QP band states have less spectral weight. At the same time the phonon distribution function in the ground state, $|c_0^m|^2$ [see Eq. (A9) in the Appendix], becomes considerably broadened,[27,51] and the position of its maximum is shifted to larger values of m. Consequently the overlap with excited multiphonon states is enlarged and the optical response is enhanced at higher energies. This redistribution of spectral weight from low to high energies can be seen in Fig. 6(c). As expected the transition to the lattice hole-polaron state, at about $\varepsilon_p^c(J=0.4,\omega_0=0.8)\simeq 2.0$, is accompanied by the development of a broad maximum in $\sigma^{\mathrm{reg}}(\omega)$, whereas the Drude weight as well as the low-frequency optical response become strongly suppressed. On the contrary, in the strong-coupling antiadiabatic regime [$\varepsilon_p=4.0,\omega_0=10.0$; see panel (d)], the low-frequency part of $\sigma^{\mathrm{reg}}(\omega)$ is much less affected, but the

optical spectrum shows additional superstructures corresponding to ''interband'' transitions between t-J–like absorption bands with different numbers of phonons.[62]

Let us now make contact with the experimentally observed characteristics of the mid-infrared spectra in the doped perovskites (for a review of the experimental and theoretical work on the optical conductivity see Refs. 63, 35, 59, and 2). Needless to say, that it is out of the scope of our ten-site cluster diagonalization study to give a quantitative theoretical description of the complex optical properties of particular copper and nickel oxides. But we would like to stress that the 2D HtJM seems to contain the key ingredients to reproduce, at least qualitatively, the principal features of the optical absorption spectra of these compounds. This can be seen by comparing the results shown in Figs. 6(b) and 6(c), which correspond to the weak and strong EP coupling situations realized in the cuprate ($La_{2-x}Sr_xCuO_4$) and nickelate ($La_{2-x}Sr_xNiO_4$) systems, respectively. The ''effective'' EP interaction ε_p/t in the nickelates is estimated to be about one order of magnitude larger than in the cuprates simply because of the much smaller transfer amplitude [$t \simeq 0.08$ eV (Ref. 16)]. According to the internal structure of the low-spin state, the hopping transport of spin-1/2 composite holes in a spin-1 background is rather complex; implying, within an effective single-band description, a strong reduction of the transition matrix elements.[64] A striking feature of the absorption spectra in the cuprate superconductors is the presence of a broad midinfrared (MIR) band, centered at about 0.5 eV in lightly doped $La_{2-x}Sr_xCuO_4$ (which, using $t \sim 0.3$ eV, means that $\omega \sim 1.5$). Such a strong MIR absorption is clearly observed in Fig. 6(b), which refers to the weak EP coupling case. Since it also appears in the pure t-J model [cf. panel (a)], this MIR band seems to be caused by the spin fluctuations around the charge carrier.[35] Obviously, it is quite difficult to distinguish the spectral weight, produced by the dressing of the hole due to the ''bag'' of reduced antiferromagnetism in its neighborhood,[65] from other (e.g., hole-phonon coupling) processes that may contribute to the MIR band observed experimentally. The results presented for the HtJM in Fig. 6(b) support the claims, however, that the MIR band in the cuprates has a mainly ''electronic'' origin, i.e., the lattice polaron effects are rather weak. The opposite is true for their isostructural counterpart, the nickelate system, where the MIR absorption band has been ascribed by many investigators to ''polaronic'' origin.[16,18] Within the HtJM such a situation can be modeled by the parameter set used in Fig. 6(c). If we fix the energy scale by $t \sim 0.08$ eV (which is the estimate for the nearest-neighbor transfer integral in $La_{2-x}Sr_xNiO_4$ given in Ref. 16), the maximum in the optical absorption is again located at about 0.5 eV. The whole spectrum clearly shows lattice polaron characteristics, where it seems that the lattice hole polarons are of small to intermediate size.[66] Most notably, we are able to reproduce the experimentally observed asymmetry in the shape of the spectrum, in particular the very gradual decay of $\sigma^{\mathrm{reg}}(\omega)$ at high energies. It is worth mentioning that this behavior cannot be obtained from a simple fit to the analytical expressions derived for the small polaron hopping conductivity.[67,68,16] Exploiting the f-sum rule we found that there are almost no contributions from bandlike carriers in agreement with the experimental findings.[16,18]

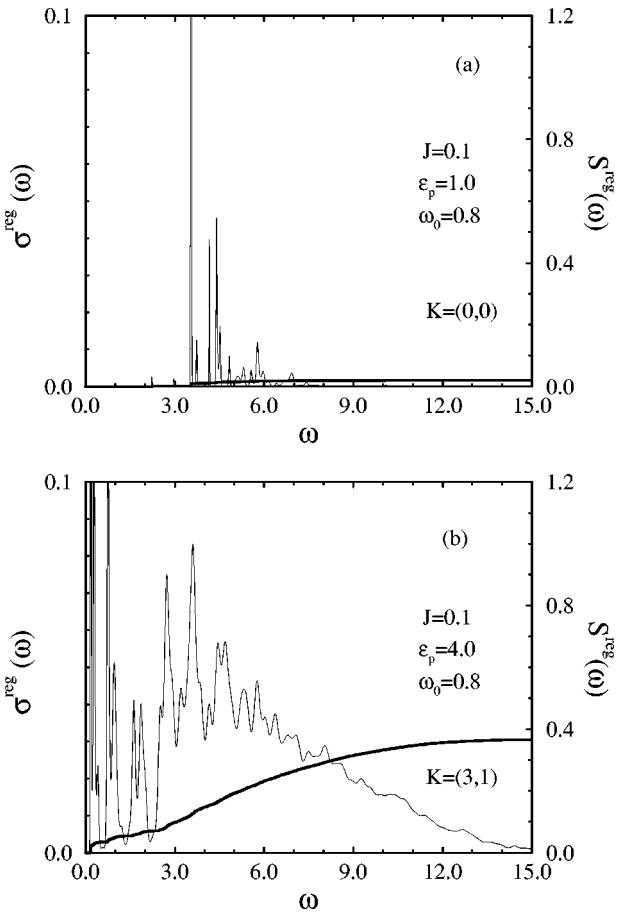

FIG. 7. Optical conductivity in the 2D HtJM for $J=0.1$ and $\omega_0=0.8$. Results are given at $\varepsilon_p=1.0$ (a) and $\varepsilon_p=4.0$ in the $\vec{K}=(0,0)$ and $\vec{K}=(3\pi/5,\pi/5)$ sectors, respectively.

Finally, we would like to consider the case $J=0.1$, which certainly has no relevance with respect to the perovskite materials but this parameter regime is interesting from a theoretical point of view. For $\varepsilon_p=0$ (t-J model), the momentum of the Nagaoka ground state is $\vec{K}=(0,0)$ and the hole can propagate without any spin scattering in the ferromagnetic background. Therefore all the spectral weight stays in the Drude pole at $\omega=0$ and the regular (incoherent) part of the optical conductivity vanishes exactly. In principle, at arbitrary small EP interactions an optical transition can be achieved by ''adding'' phonons with momentum $(-\vec{K})$ to band states $E_{\vec{K}}$ [in order to reach the $\vec{K}=(0,0)$ sector]. However, the overlap of these excited states with the almost zero-phonon ground state is extremely small and, as a direct consequence, $S^{\mathrm{reg}}(\infty)$ is negligible [see Fig. 7(a)]. A completely different situation arises when the charge carrier becomes ''self-trapped'' due to the lattice distortions. When the lattice hole-polaron formation takes place, the momentum of the ground state of the 2D ten-site HtJM is switched from (0,0) to $\vec{K}=(3\pi/5,\pi/5)$ and, what is more important, the AFM exchange interaction becomes more effective. This gives rise to the pronounced low-frequency peak structures found in Fig. 7(b), which are originated from spin excitations on an energy scale of the order of J. At higher energies we recover the characteristic features of the lattice hole-polaron spectrum discussed in Fig. 6(c).

VI. SUMMARY

We have investigated the spectral properties of the two-dimensional Holstein *t-J* model as a generic model for studying polaronic effects in systems with strong Coulomb correlations. The use of purely numerical techniques allows one to treat the electron and phonon degrees of freedom on an equal footing. In the numerical work the full dynamics of all the phonon modes was taken into account on finite lattices with up to 16 sites. The efficiency and accuracy of the employed phonon Hilbert space truncation, Lanczos diagonalization, Chebyshev recursion, and maximum entropy methods have been demonstrated in the Appendix.

In conclusion, we have shown that an additional hole-phonon coupling strongly affects the nature of the quasiparticle excitations and the charge-carrier transport in the 2D *t-J* model. Our results indicate that the magnetic prelocalization of the holes, due to strong spin correlations, strengthens the effect of the hole-phonon interaction. Thus the tendency towards lattice (hole) polaron formation is enhanced in strongly correlated electron systems.

The wave-vector resolved single hole spectral function yields a flattening of the coherent band dispersion in the vicinity of the band maxima for the adiabatic weak and intermediate hole-phonon coupling cases. As the hole-phonon interaction increases, a narrow lattice hole-polaron band separates from the rest of the spectrum but the spectral weight of these quasiparticle band states becomes more and more suppressed. In the antiadiabatic regime the low-energy excitations of the *t-J* model are less affected by the hole-phonon interaction; at higher energies we found ''interband'' transitions corresponding to multiphonon absorption processes.

The formation of lattice hole polarons is accompanied by significant changes in the optical response of the system. Both the coherent Drude part and the low-frequency regular contribution to the optical conductivity are strongly reduced and, concomitantly, we observe a substantial spectral weight transfer to higher energies. In the intermediate-to-strong hole-phonon coupling regimes, i.e., in the vicinity of the lattice hole-polaron transition, the line shape of the optical absorption spectra is highly asymmetric with a long incoherent tail at high frequencies, which also seems to be in accordance with recent mid- and far-infrared optical experiments on $La_{2-x}Sr_xNiO_4$.[16,18] The present calculations point toward the importance of strong spin correlation and polaronic effects in explaining the origin of the anomalous midinfrared absorption band observed in the cuprate and nickelate compounds, respectively. Of course, for a realistic modeling of the complex high-spin low-spin nickelate system, one has to take into account more complicated hopping and spin exchange processes. Work along this line is in progress.

ACKNOWLEDGMENTS

This work was performed under the auspices of Deutsche Forschungsgemeinschaft, through SFB 279. Special thanks go to the LRZ München, the HLRZ Jülich, and HLR Stuttgart for the generous granting of their parallel computer facilities. We have benefited from discussions with A. Basermann, A. R. Bishop, H. Büttner, D. Ihle, J. Loos, and H. Röder. We are particularly indebted to R. N. Silver for putting his maximum entropy code at our disposal.

APPENDIX: NUMERICAL METHODS

Symmetrized basis and Hilbert space truncation

1. Basis symmetrization. The total Hilbert space of the HtJM can be written as the tensorial product space of electrons and phonons, spanned by the complete basis set

$$\{|\Phi_{uv}\rangle = |u\rangle_{\rm el} \otimes |v\rangle_{\rm ph}\} \tag{A1}$$

with

$$|u\rangle_{\rm el} = \prod_{i=1}^{N} \prod_{\sigma=\uparrow,\downarrow} (\tilde{c}_{i\sigma}^{\dagger})^{n_{i\sigma,u}} |0\rangle_{\rm el}, \quad n_{i\sigma,u} \in \{0,1\}, \tag{A2}$$

$$|v\rangle_{\rm ph} = \prod_{i=1}^{N} \frac{1}{\sqrt{m_{i,v}!}} (b_i^{\dagger})^{m_{i,v}} |0\rangle_{\rm ph}, \quad m_{i,v} \in \{0,\ldots,\infty\}. \tag{A3}$$

Here $u=1,\ldots,D_{\rm el}$ and $v=1,\ldots,D_{\rm ph}$ label the basic states of the electronic and phononic subspaces with dimensions $D_{\rm el}=\binom{N}{N_\sigma}\binom{N-N_\sigma}{N_{-\sigma}}$ and $D_{\rm ph}=\infty$, respectively.

Since the Hamiltonian (1) commutes with the electron number operator $\mathcal{N}_{\rm el}=\sum_{i=1}^{N}(\tilde{n}_{i,\uparrow}+\tilde{n}_{i,\downarrow})$ and the z component of the total spin $\mathcal{S}^z=\frac{1}{2}\sum_{i=1}^{N}(\tilde{n}_{i,\uparrow}-\tilde{n}_{i,\downarrow})$ the basis (A1) has been constructed for fixed $N_h=N-N_{\rm el}$ and $S^z=S^z_{\rm min}$. To further reduce the dimension of the total Hilbert space, we can exploit the space-group symmetries [translations (G_T) and point group operations (G_L)] and the spin-flip invariance [(G_S); $S^z=0$ subspace only]. Clearly, working on finite bipartite clusters ($N=k^2+l^2$, k and l are both even or odd integers) with periodic boundary conditions, we do not have all the symmetry properties of the 2D square lattice. Restricting ourselves to the one-dimensional non-equivalent irreducible representations of the group $G(\vec{K})=G_T\times G_L(\vec{K})\times G_S$, we can use the projection operator

$$\mathcal{P}_{\vec{K},rs} = \frac{1}{g(\vec{K})} \sum_{\mathcal{G}\in G(\vec{K})} \chi^{(\mathcal{G})}_{\vec{K},rs} \mathcal{G} \tag{A4}$$

(with $[\mathcal{H},\mathcal{P}_{\vec{K},rs}]=0$, $\mathcal{P}^{\dagger}_{\vec{K},rs}=\mathcal{P}_{\vec{K},rs}$ and $\mathcal{P}_{\vec{K},rs}\mathcal{P}_{\vec{K}',r's'}=\mathcal{P}_{\vec{K},rs}\delta_{\vec{K},\vec{K}'}\delta_{r,r'}\delta_{s,s'}$), in order to generate a new symmetrized basis set: $\{|\Phi_{uv}\rangle\}\xrightarrow{\mathcal{P}}\{|\tilde{\Phi}_{\tilde{u}v}\rangle\}$. In Eq. (A4), $\mathcal{G}$ denotes the $g(\vec{K})$ elements of the group $G(\vec{K})$ and $\chi^{(\mathcal{G})}_{\vec{K},rs}$ is the (complex) character of $\mathcal{G}$ in the $[\vec{K},rs]$ representation, where $\vec{K}$ refers to one of the N allowed wave vectors in the first Brillouin zone, r labels the irreducible representations of the little group of $\vec{K}$, $G_L(\vec{K})$, and s parametrizes G_S. For an efficient parallel implementation of the matrix vector multiplications (MVM) required diagonalizing the Hamiltonian, it is extremely important that the symmetrized basis can be constructed preserving the tensor product structure of the Hilbert space:

$$\{|\tilde{\Phi}_{\tilde{u}v}\rangle = N^{[\vec{K}rs]}_{\tilde{u}v} \mathcal{P}_{\vec{K},rs}[|\tilde{u}\rangle_{\rm el} \otimes |v\rangle_{\rm ph}]\}. \tag{A5}$$

Here $\tilde{u}=1,\ldots,\tilde{D}_{\rm el}^{g(\vec{K})}$ $[\tilde{D}_{\rm el}^{g(\vec{K})}\sim D_{\rm el}/g(\vec{K})]$, and the $N^{[\vec{K}rs]}$ are normalization factors.

2. Phonon Hilbert space truncation. Since the Hilbert space associated to the phonons is infinite even for a finite system, we apply a truncation procedure[69,27] retaining only basis states with at most M phonons:

$$\left\{ |v\rangle_{\rm ph};\ m_v=\sum_{i=1}^{N} m_{i,v}\leqslant M \right\}. \tag{A6}$$

The resulting Hilbert space has a total dimension $\tilde{D}^M=\tilde{D}_{\rm el}^{g(\vec{K})}\times D_{\rm ph}^M$ with $D_{\rm ph}^M=(M+N)!/M!N!$, and a general state of the HtJM is represented as

$$|\Psi_{\vec{K},rs}\rangle=\sum_{\tilde{u}=1}^{\tilde{D}_{\rm el}^{g(\vec{K})}}\sum_{v=1}^{D_{\rm ph}^M}\tilde{c}_{\tilde{u}v}|\tilde{\Phi}_{\tilde{u}v}\rangle. \tag{A7}$$

It is worthwhile to point out that, switching from a real space representation to a momentum space description, our truncation scheme takes into account *all* dynamical phonon modes. This has to be contrasted with the frequently used single-mode approaches.[34,70] In other words, depending on the model parameters and the band filling, the system ''decides'' by itself how the M phonons will be distributed among the independent Einstein oscillators related to the N Wannier sites or, alternatively, among the N different phonon modes in $\vec{Q}$ space. Hence with the same accuracy phonon dynamical effects on lattice distortions being quasilocalized in real space (such as polarons, Frenkel excitons, etc.) or in momentum space (like polaronic superlattices, charge-density waves, etc.) can be studied.

Of course, one has to carefully check for the convergence of the above truncation procedure by calculating the ground-state energy as a function of the cutoff parameter M. In the numerical work convergence is assumed to be achieved if E_0 is determined with a relative error

$$\Delta E_0^{(M)}=\frac{E_0(M)-E_0(M-1)}{E_0(M)}\leqslant 10^{-6}. \tag{A8}$$

In addition we guarantee that the phonon distribution function

$$|c^{(m)}|^2(M)=\sum_{\tilde{u}=1}^{\tilde{D}_{\rm el}^{g(\vec{K})}}\sum_{\substack{v=1\\ \{m_v=m\}}}^{D_{\rm ph}^M}|\tilde{c}_{\tilde{u}v}|^2, \tag{A9}$$

which gives the different weights of the m-phonon states in the ground state $|\Psi_0\rangle$, becomes independent of M and $|c^{(M)}|^2(M)\leqslant 10^{-6}$.

To illustrate the M dependences of the phonon distribution function and the ground-state energy, we have shown both quantities in Fig. 8 for the HtJM with $\varepsilon_p=4.0$, $\hbar\omega_0=0.8$, and $J=0.4$. Figure 8 proves that our truncation procedure is very well controlled even in the strong EP coupling regime, where multiphonon states become increasingly important. Although not mentioned each time, all the results presented in this paper have been obtained with a sufficiently large value of M ensuring the above convergence criteria for both static (ground state) and dynamic (excited state) properties.

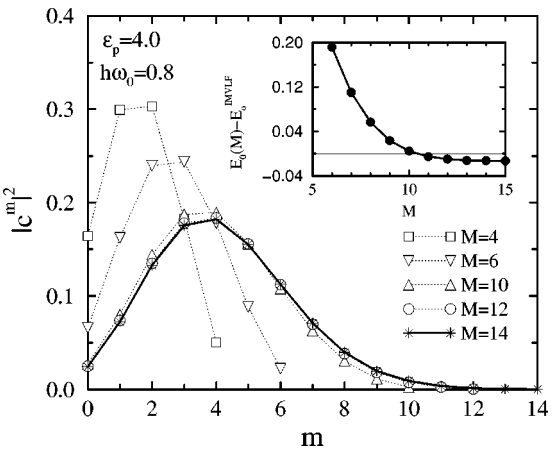

FIG. 8. Convergence of the phonon distribution function $|c^m|^2(M)$ and ground-state energy $E_0(M)$ (inset) as a function of the maximum number of phonons M for the 2D HtJM on a ten-site lattice ($J=0.4$). $E_0(M)$ is given with respect to the variational estimate of ground-state energy, $E_0^{(\rm IMVLF)}$, obtained within the IMVLF-Lanczos approach developed recently by the authors (Ref. 26).

Finally we would like to stress that it is not possible to keep all nonvanishing matrix elements of our ten-site Holstein t-J Hamiltonian in the memory of the present day parallel computers because, in spite of applying the symmetrization and Hilbert space truncation procedures, the total dimension of the problem is still very large. Therefore, performing the matrix-vector operations, we create the nonzero matrix elements of the Hamiltonian simultaneously. For the example considered in Fig. 8, we have $\tilde{D}^M=4.12\times 10^8$ ($M=15$) phonons, and each MVM takes about 100 sec CPU time on a CRAY T3E with 126 processors.

Algorithms for estimating spectral functions

The numerical calculation of spectral functions,

$$A^{\mathcal{O}}(\omega)=-\lim_{\varepsilon\to 0^+}\frac{1}{\pi}{\rm Im}\left[\langle\Psi_0|\mathbf{O}^\dagger\frac{1}{\omega-\mathbf{H}+E_0+i\varepsilon}\mathbf{O}|\Psi_0\rangle\right]$$
$$=\sum_{n=0}^{D-1}|\langle\Psi_n|\mathbf{O}^\dagger|\Psi_0\rangle|^2\delta[\omega-(E_n-E_0)], \tag{A10}$$

where $\mathbf{O}$ is the matrix representation of a certain operator $\mathcal{O}$ [e.g., the destruction operator $\tilde{c}_{\vec{K},\sigma}$ of an electron with momentum $\vec{K}$ and spin σ if one wants to calculate the single hole spectral function (2)], involves very large sparse Hamilton matrices $\mathbf{H}$. For example, for the EP systems studied in this paper, we have calculated spectral properties of the HtJM acting in Hilbert spaces with total dimensions up to $D=10^9$. Finding all (D) eigenvectors and eigenstates of such huge Hamiltonian matrices is impossible, because the CPU time required for exact diagonalization of $\mathbf{H}$ scales as D^3 and memory as D^2. Fortunately, there exist very accurate and well-conditioned linear scaling algorithms for a direct approximate calculation of $A^{\mathcal{O}}(\omega)$.

In this appendix we compare the widely used *spectral decoding method* (SDM),[71] which is a refinement of the standard *Lanczos recursion method* (LRM),[72] with two more recent Chebyshev recursion techniques, the *kernel polynomial method*[73] (KPM) and the *maximum entropy method* (MEM).[74] To come to the conclusion first, the MEM is found to be the most efficient and numerically stable method for high-energy resolution applications such as the lattice polaron formation problem.

In the following we briefly review the basics of the SDM, KPM, and MEM (for a more detailed discussion see, e.g., Refs. 35 and 73–75), and illustrate their efficiency and accuracy with several examples.

1. SDM. First one calculates by iterative matrix-on-vector multiplications,

$$|\bar{\Phi}_{l+1}\rangle = \mathbf{H}^D|\bar{\Phi}_l\rangle - \frac{\langle\bar{\Phi}_l|\mathbf{H}^D|\bar{\Phi}_l\rangle}{\langle\bar{\Phi}_l|\bar{\Phi}_l\rangle}|\bar{\Phi}_l\rangle - \frac{\langle\bar{\Phi}_l|\bar{\Phi}_l\rangle}{\langle\bar{\Phi}_{l-1}|\bar{\Phi}_{l-1}\rangle}|\bar{\Phi}_{l-1}\rangle, \tag{A11}$$

a *tridiagonal* matrix $[\mathbf{T}^L]_{l,l'} = \langle\bar{\Phi}_l|\mathbf{H}^D|\bar{\Phi}_{l'}\rangle$ with dimension $L \ll D$, starting out from $|\bar{\Phi}_1\rangle = \mathbf{H}^D|\bar{\Phi}_0\rangle - \langle\bar{\Phi}_0|\mathbf{H}^D|\bar{\Phi}_0\rangle/\langle\bar{\Phi}_0|\bar{\Phi}_0\rangle|\bar{\Phi}_0\rangle$, where $\mathbf{H}^D$ denotes the Hamilton matrix acting in a D-dimensional Hilbert space and $|\bar{\Phi}_0\rangle$ is an arbitrary initial state having finite overlap with the true ground state $|\Psi_0\rangle$. Applying the Lanczos recursion (A11), the eigenvalues E_n and eigenvectors $|\Psi_n\rangle$ of $\mathbf{H}^D$ are approximated by those of $\mathbf{T}^L$,[76] E_n^L and $|\Psi_n^L\rangle = \Sigma_{l=0}^{L-1} c_{n,l}^L|\bar{\Phi}_l\rangle$, respectively.

Then, having determined the ground state $|\Psi_0^L\rangle$ by the Lanczos technique, we can use again the recursion relation (A11), but with the initial state

$$|\bar{\Phi}_0\rangle = \frac{\mathbf{O}|\Psi_0^L\rangle}{\sqrt{\langle\Psi_0^L|\mathbf{O}^\dagger\mathbf{O}|\Psi_0^L\rangle}}, \tag{A12}$$

to determine within the SDM an approximative spectral function,

$$\bar{A}^{\mathcal{O}}(\omega) = \sum_{n=0}^{L-1} |c_{n,0}^L|^2\langle\Psi_0|\mathbf{O}^\dagger\mathbf{O}|\Psi_0\rangle\,\delta[\omega-(E_n^L-E_0^L)], \tag{A13}$$

built up by L δ peaks. Of course, the true spectral function $A^{\mathcal{O}}(\omega)$ has D δ peaks. According to the Lanczos phenomenon the approximated spectral weights and positions of the peaks converge to their true values with increasing L. Some of the main problems of the SDM/LRM are as follows: (i) The convergence is not uniform in the whole energy range. (ii) There exist so-called spurious peaks, which appear and disappear as L is increased, i.e., when the iteration proceeds. (iii) Without computationally expensive reorthogonalization only a few hundred iterations are possible.

2. KPM and MEM. The idea behind the Chebyshev recursion methods is to expand the δ-function contained in $A(\omega)$ in a series of Chebyshev polynomials $T_m(x)$,

$$A^{\mathcal{O}}(x) = \frac{1}{\pi\sqrt{1-x^2}}\left(\mu_0^{\mathcal{O}} + 2\sum_{m=1}^{\infty}\mu_m^{\mathcal{O}}T_m(x)\right), \tag{A14}$$

with the coefficients (moments)

$$\mu_m^{\mathcal{O}} = \int_{-1}^{1} dx\,T_m(x)A^{\mathcal{O}}(x) = \langle\mathbf{O}^\dagger\Psi_0|T_m(\mathbf{X})|\mathbf{O}^\dagger\Psi_0\rangle, \tag{A15}$$

$x=(\omega-b)/a$, $a=(E_{\max}-E_{\min})/2(1-\epsilon)$, and $b=(E_{\max}+E_{\min})/2$. Since the Chebyshev polynomials are defined on the interval $[-1,1]$, a rescaled Hamiltonian $\mathbf{X}=(\mathbf{H}-b)/a$ has to be considered, whose eigenvalues x_n are in the range $[-(1-\epsilon),1-\epsilon]$. Here a small constant ϵ is introduced in order to avoid convergence problems at the endpoints of the interval (a typical choice is $\epsilon\sim 0.01$, which has only 1% impact on the energy resolution[74]). The $\mu_m^{\mathcal{O}}$ can be easily computed by iterative MVM. Truncating the expansion (A14) at $\mu_{\widetilde{M}}^{\mathcal{O}}$, the main difference between KPM and MEM is the way the spectral function is reconstructed from the remaining $\widetilde{M}$ moments.

The KPM is a *linear* Chebyshev approximation to the spectrum, $\widetilde{A}^{\mathcal{O}}(x) \simeq A^{\mathcal{O}}(x)$, using $\widetilde{M}$ moments only. Here the abrupt truncation of the series produces the well-known Gibbs oscillations which, however, can be minimized by multiplying the moments by appropriate damping factors.[77]

On the other hand, the MEM is a *nonlinear* optimization procedure for calculating from the $\hat{M}$ known moments a representation of a (reconstructed) spectral function, $\hat{A}^{\mathcal{O}}(\phi) = \check{A}^{\mathcal{O}}(x)\sin\phi$ with $x=\cos\phi$, that corresponds to a Chebyshev series with $\hat{M}^{\text{eff}} = F\hat{M}$ summands. The $\hat{M}^{\text{eff}}$ moments

$$\hat{\mu}_m^{\mathcal{O}} = \int_0^{\pi} d\phi\cos(m\phi)\hat{A}^{\mathcal{O}}(\phi), \tag{A16}$$

are determined by maximizing the information theoretical relative entropy[74]

$$\mathcal{S} = \int_0^{\phi} d\phi\left[\hat{A}^{\mathcal{O}}(\phi) - \hat{A}_0^{\mathcal{O}}(\phi) - \hat{A}^{\mathcal{O}}(\phi)\ln\left(\frac{\hat{A}^{\mathcal{O}}(\phi)}{\hat{A}_0^{\mathcal{O}}(\phi)}\right)\right] \tag{A17}$$

subject to the constraint that the first $\hat{M}$ moments of $\hat{A}^{\mathcal{O}}(\phi)$ are equal to the $\hat{M}$ known moments. $\hat{A}_0^{\mathcal{O}}(\phi)$ is a default model for $\hat{A}^{\mathcal{O}}(\phi)$. We choose the KPM result $\check{A}_0^{\mathcal{O}}(x) = \widetilde{A}^{\mathcal{O}}(x)$. F is typically $8, \ldots, 32$.

For the MEM (KPM) the calculation of the Chebyshev moments and not the reconstruction of the spectral function requires the essential part of CPU time and memory. Clearly this is because in moment production MVM with $\mathbf{H}^D$ is involved, whereas the reconstruction of the spectrum only processes the $\widetilde{M}$ ($\hat{M}$) moments.

In the numerical work we used the following algorithm producing two moments per MVM with $\mathbf{H}^D$: (i) Determine from Lanczos diagonalization the ground state $|\Psi_0\rangle$ and the extreme eigenvalues $E_{\min}=E_0$ and $E_{\max}$ of $\mathbf{H}^D$. (ii) Compute the starting conditions

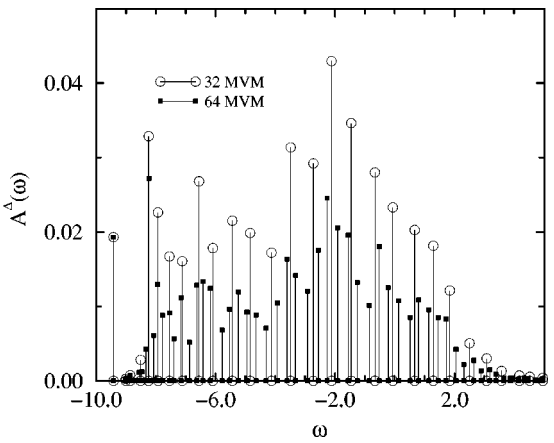

FIG. 9. Dynamical d-wave pair correlation function of the pure 2D t-J model, $A^{\Delta}(\omega)=\Sigma_n|\langle\Psi_n^{(N-2)}|\Delta|\Psi_0^{(N)}\rangle|^2\delta[\omega-(E_n^{(N-2)}-E_0^{(N)})]$, where $\Delta=(1/\sqrt{N})\Sigma_{i,\delta=\pm}\tilde{c}_{i\uparrow}(\tilde{c}_{i+\delta x\downarrow}-\tilde{c}_{i+\delta y\downarrow})$. Results are calculated on a 16-site lattice with two holes for $J=0.3$ using SDM with $L=32$ and 64 MVM.

$$|\hat{\Phi}_0\rangle=\mathbf{O}^{\dagger}|\Psi_0\rangle,\quad |\hat{\Phi}_1\rangle=\mathbf{X}|\hat{\Phi}_0\rangle, \tag{A18}$$

$$\mu_0^{\mathcal{O}}=\langle\hat{\Phi}_0|\hat{\Phi}_0\rangle,\quad \mu_1^{\mathcal{O}}=\langle\hat{\Phi}_0|\hat{\Phi}_1\rangle. \tag{A19}$$

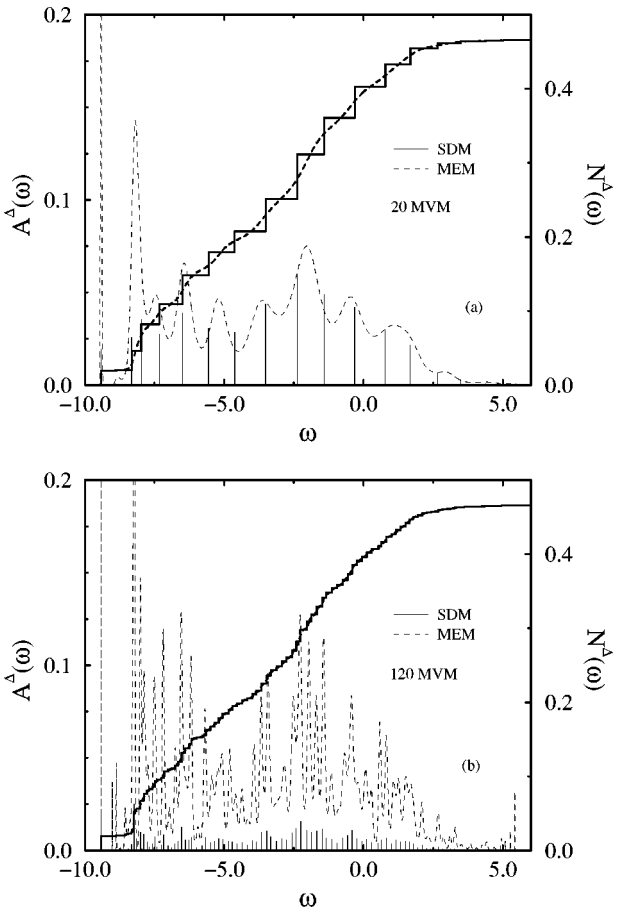

FIG. 10. SDM (thin solid lines) and MEM (thin dashed lines) results obtained for the pair correlation function $A^{\Delta}(\omega)$ in the 2D t–J model with 20 (a) and 120 MVM (b) [$J=0.3$, $N=16$]. Shown is also the corresponding integrated spectral weight $N^{\Delta}(\omega)=\int_{-\infty}^{\omega}d\omega' A^{\Delta}(\omega')$ (bold lines).

(iii) Use the recurrence relations for Chebyshev polynomials to calculate the $\hat{M}$ moments according to

$$|\hat{\Phi}_m\rangle=2\mathbf{X}|\hat{\Phi}_{m-1}\rangle-|\hat{\Phi}_{m-2}\rangle, \tag{A20}$$

$$\mu_{2m}^{\mathcal{O}}=2\langle\hat{\Phi}_m|\hat{\Phi}_m\rangle-\mu_0^{\mathcal{O}}, \tag{A21}$$

$$\mu_{2m-1}^{\mathcal{O}}=2\langle\hat{\Phi}_m|\hat{\Phi}_{m-1}\rangle-\mu_1^{\mathcal{O}}. \tag{A22}$$

Note that applying this procedure only two D-dimensional vectors have to be stored. The algorithm is numerically very stable, so in contrast to the SDM/LRM (continued fraction based technique[35]) thousands of Chebyshev moments can be calculated with satisfying accuracy.

3. Examples. Figure 9 demonstrates the nonuniform convergence of the SDM/LRM for the dynamical pair correlation spectrum of the t-J model (for a discussion of the physics described by $A^{\Delta}(\omega)$ see, e.g., Refs. 35 and 78). Obviously, we found a much faster convergence in the low-energy regime. Increasing L the peak resolution becomes better at higher energies as well, but now one is confronted with the reorthogonalization problem mentioned above.

Another typical problem concerns the proper description of gap structures. As can be seen from Fig. 10(a), the gap located at the bottom of the spectrum of the d-wave pair correlator cannot be identified using SDM with $L=20$ MVM only, because the averaged distance between two (SDM) δ peaks (vertical lines) is of the same order of magnitude. Thus the true gap structure of the spectrum remains hidden. By choosing the MEM, one obtains a smooth reconstruction of the whole spectrum and achieves a significant better resolution of the gap from the same number of MVM. This becomes particularly obvious by looking at the ω-integrated

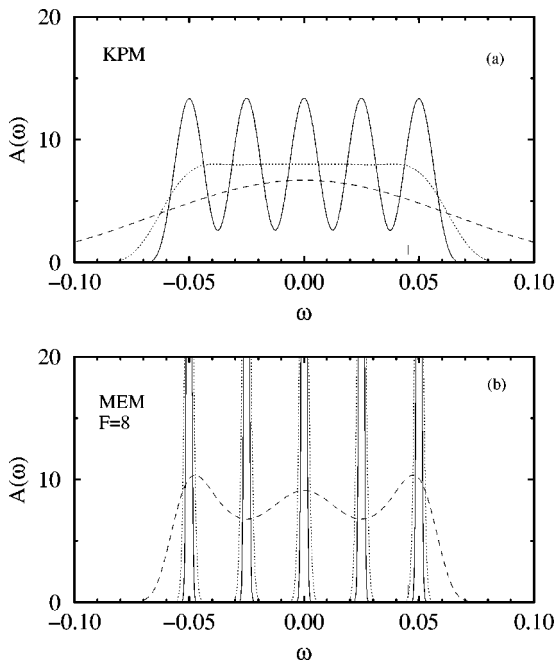

FIG. 11. Comparison of KPM (a) and MEM (b) by means of a fictitious spectrum consisting of five δ peaks. The reconstructed spectral function is shown using 64 (dashed), 256 (dotted), and 512 (solid) moments.

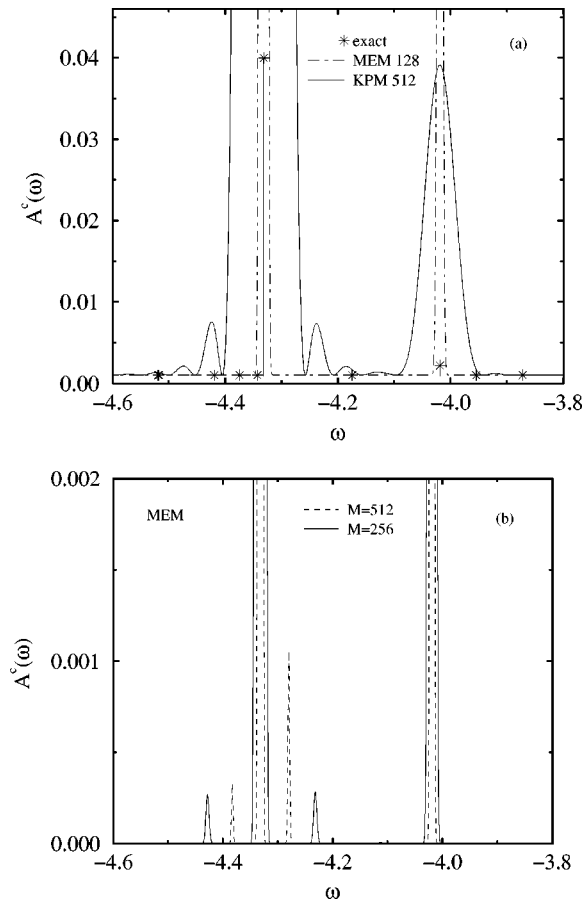

FIG. 12. Depicted is a part of the excitation spectrum of a single hole with momentum $\vec{K}=(3,1)\pi/5$ in the 2D t-J model ($D=126$). In upper panel, the KPM and MEM reconstructed spectral function $\tilde{A^c}(\omega)$ has been calculated using 512 and 128 moments, respectively. For comparison the exact peak positions and spectral weights are shown (stars). In the lower panel we illustrate how spurious peaks can be identified.

spectral function $N^{\Delta}(\omega)$. In $N^{\Delta}(\omega)$ the dominant low-energy QP peak (corresponding to the jumplike behavior of $N^{\Delta}(\omega)$ at the bottom of the spectrum) is clearly separated from the incoherent high-energy part by an energy gap [with $N^{\Delta}(\omega) \simeq$const]. Of course, for both methods the energy resolution gets better with increasing number of moments [see Fig. 10(b)], and consequently the SDM and MEM results converge on each other. However, since the dimension of the Hilbert space ($D=10^3$) is rather small for the spectra shown in Fig. 10(b), we have calculated about 10% of the true peaks by using 120 MVM (on the other hand, for our EP systems having a total dimension of 10^9 this corresponds to only 10^{-7} of the possible excitations). Most notably, the spectral weight of different parts of the MEM spectrum does not change any more going from 20 to 120 MVM.

Since for any finite system the true spectral function will consist of a sum of delta functions, we compare the efficiency of KPM and MEM in dependence of the number of moments by reconstructing a fictitious reference spectrum of five δ peaks. Figure 11 demonstrates that the MEM provides a dramatic improvement in energy resolution over the KPM (typically by a factor of 4). Thus the spectral function is much better reconstructed, in particular when the number of MVM is small. On the other hand, an advantage of the linear KPM over nonlinear MEM is that the KPM smoothing is uniquely determined by the number of Chebyshev recursions,[77] i.e., in contrast to the MEM we have a uniform energy resolution $\propto \tilde{M}^{-1}$.

To analyze the accuracy of the KPM and MEM in more detail we have compared in Fig. 12 a portion of a reconstructed single hole spectrum with the true spectral function obtained without moment truncation, i.e., from the full diagonalization of the system. Again convergence to the exact data is seen to be more rapid by applying the MEM (note that $\tilde{M}=4\hat{M}$). Moreover, the peaks in the KPM spectra are surrounded by not fully damped Gibbs oscillations. As can be seen from Fig. 12(b), the MEM produces artificial peaks as well but they are at least one order of magnitude smaller than those for KPM. That means that these isolated spurious eigenvalues have extremely small spectral weight and hence negligible influence on the cumulative spectrum. To illustrate that these spurious peaks can be easily identified, we have plotted the MEM spectrum for different number of moments. Contrary to the true eigenvalues the spurious peaks (often labeled ''ghosts'') move about as $\hat{M}$ increases.

[1] Y. Bar-Yam, T. Egami, J. M. de Leon, and A. R. Bishop, *Lattice Effects in High-T_c Superconductors* (World Scientific, Singapore, 1992).

[2] E. K. H. Salje, A. S. Alexandrov, and W. Y. Liang, *Polarons and Bipolarons in High Temperature Superconductors and Related Materials* (Cambridge University Press, Cambridge, 1995).

[3] C. H. Chen, S.-W. Cheong, and A. S. Cooper, Phys. Rev. Lett. **71**, 2461 (1993).

[4] A. J. Millis, P. B. Littlewood, and B. I. Shraiman, Phys. Rev. Lett. **74**, 5144 (1995).

[5] T. Egami, D. Louca, and R. J. McQueeney, J. Supercond. **10**, 323 (1997).

[6] J. M. Tranquada, B. J. Sternlieb, J. D. Axe, Y. Nakamura, and S. Uchida, Nature (London) **375**, 561 (1995).

[7] G. Zhao, K. Conder, H. Keller, and K. A. Müller, Nature (London) **381**, 676 (1996).

[8] J. M. Tranquada, Physica C **282-287**, 166 (1997).

[9] A. Bianconi, N. L. Saini, A. Lanzara, M. Missori, T. Rossetti, H. Oyanagi, H. Yamaguchi, K. Ota, and T. Ito, Phys. Rev. Lett. **76**, 3412 (1996).

[10] S.-W. Cheong, H. Y. Hwang, C. H. Chen, B. Batlogg, L. W. Rupp, Jr., and S. A. Carter, Phys. Rev. B **49**, 7088 (1994).

[11] J. M. Tranquada, D. J. Buttrey, V. Sachan, and J. E. Lorenzo, Phys. Rev. Lett. **73**, 1003 (1994).

[12] M. von Zimmermann, A. Vigliante, T. Frello, J. Madsen, D. J. Buttrey, N. H. Andersen, J. R. Schneider, Doon Gibbs, and J. M. Tranquada, J. Supercond. **10**, 447 (1997).

[13] D. Louca, T. Egami, E. L. Brosha, H. Röder, and A. R. Bishop, Phys. Rev. B **56**, R8475 (1997).

[14] D. N. Argyriou, J. F. Mitchell, C. D. Potter, D. G. Hinks, J. D. Jorgensen, and S. D. Bader, Phys. Rev. Lett. **76**, 3826 (1996).

[15] S.-H. Lee and S.-W. Cheong, Phys. Rev. Lett. **79**, 2514 (1997).

[16] X.-X. Bi and P. C. Eklund, Phys. Rev. Lett. **70**, 2625 (1993).
[17] P. Calvani, A. Paolone, P. Dore, S. Lupi, P. Maselli, P. G. Medaglia, and S.-W. Cheong, Phys. Rev. B **54**, R9592 (1996).
[18] P. Calvani, P. Dore, S. Lupi, A. Palone, P. Maselli, P. Giura, B. Ruzicka, S.-W. Cheong, and W. Sadowski, J. Supercond. **10**, 293 (1997).
[19] D. Emin, Phys. Rev. B **48**, 13 691 (1993).
[20] D. Mihailović, C. Stevens, J. Demsar, B. Podobnik, D. C. Smith, and J. F. Ryan, J. Supercond. **10**, 753 (1997).
[21] A. Ramšak, P. Horsch, and P. Fulde, Phys. Rev. B **46**, 14 305 (1992).
[22] B. Kyung, S. I. Mukhin, V. N. Kostur, and R. A. Ferrell, Phys. Rev. B **54**, 13 167 (1996).
[23] L. Pietronero, S. Strässler, and C. Grimaldi, Phys. Rev. B **52**, 10 516 (1995).
[24] C. Grimaldi, L. Pietronero, and S. Strässler, Phys. Rev. B **52**, 10 530 (1995).
[25] C. Grimaldi, E. Cappelluti, and L. Pietronero, cond-mat/9710159 (unpublished).
[26] H. Fehske, H. Röder, G. Wellein, and A. Mistriotis, Phys. Rev. B **51**, 16 582 (1995).
[27] G. Wellein, H. Röder, and H. Fehske, Phys. Rev. B **53**, 9666 (1996).
[28] S. Ishihara, T. Egami, and M. Tachiki, Phys. Rev. B **55**, 3163 (1997).
[29] T. Sakai, D. Poilblanc, and D. J. Scalapino, Phys. Rev. B **55**, 8445 (1997).
[30] A. N. Das, J. Konior, and D. K. Ray, Physica C **170**, 215 (1990).
[31] H. Fehske, H. Röder, A. Mistriotis, and H. Büttner, J. Phys.: Condens. Matter **5**, 3635 (1993).
[32] R. Fehrenbacher, Phys. Rev. B **49**, 12 230 (1994).
[33] A. Sherman and M. Schreiber, Phys. Rev. B **52**, 10 621 (1995).
[34] D. Poilblanc, T. Sakai, D. J. Scalapino, and W. Hanke, Europhys. Lett. **34**, 367 (1996).
[35] E. Dagotto, Rev. Mod. Phys. **66**, 763 (1994).
[36] In recent Hubbard or *t-J* model studies the term ''hole polaron'' has become popular for denoting the hole QP dressed by *magnons*, i.e., for a *magnetic* polaron. In order to avoid confusion, throughout this work we specify the otherwise standard notation ''polaron'' as *lattice* (hole) polaron, whenever the hole-phonon coupling effects are dominating.
[37] U. Trapper, H. Fehske, M. Deeg, and H. Büttner, Z. Phys. B **93**, 465 (1993).
[38] H. Fehske, D. Ihle, J. Loos, U. Trapper, and H. Büttner, Z. Phys. B **94**, 91 (1994).
[39] H. Fehske and M. Deeg, Physica C **235-240**, 2243 (1994).
[40] A. Sherman, J. Sabczynski, and M. Schreiber, Z. Phys. B **84**, 343 (1991).
[41] A. Sherman, J. Sabczynski, and M. Schreiber, Phys. Lett. A **195**, 231 (1994).
[42] J. Zhong and H.-B. Schütter, Phys. Rev. Lett. **69**, 1600 (1992).
[43] H. Röder, H. Fehske, and H. Büttner, Phys. Rev. B **47**, 12 420 (1993).
[44] H. Röder, H. Fehske, and R. N. Silver, Europhys. Lett. **28**, 257 (1994).
[45] R. Fehrenbacher, Phys. Rev. Lett. **77**, 2288 (1996).
[46] G. Wellein, H. Fehske, H. Büttner, and A. R. Bishop, Physica C **282-287**, 1827 (1997).
[47] A. Dobry, A. Greco, S. Koval, and J. Riera, Phys. Rev. B **52**, 13 722 (1995).
[48] W. Brenig, Phys. Rep. **251**, 153 (1995).
[49] D. Poilblanc, T. Ziman, H. J. Schulz, and E. Dagotto, Phys. Rev. B **47**, 14 267 (1993).
[50] H. Fehske, J. Loos, and G. Wellein, Z. Phys. B **104**, 619 (1997).
[51] H. Fehske, G. Wellein, B. Bäuml, and H. Büttner, Physica B **230-232**, 899 (1997).
[52] E. Dagotto, R. Joynt, A. Moreo, S. Bacci, and E. Gagliano, Phys. Rev. B **41**, 9049 (1990).
[53] R. Eder, K. W. Becker, and W. H. Stephan, Z. Phys. B **81**, 33 (1990).
[54] G. Martinez and P. Horsch, Int. J. Mod. Phys. B **5**, 207 (1991).
[55] W. Stephan, Phys. Rev. B **54**, 8981 (1996).
[56] G. Wellein and H. Fehske, Phys. Rev. B **56**, 4513 (1997).
[57] B. S. Shastry and B. Sutherland, Phys. Rev. Lett. **65**, 243 (1990).
[58] G. C. Psaltakis, J. Phys.: Condens. Matter **8**, 5089 (1996).
[59] A. S. Alexandrov, V. V. Kabanov, and D. K. Ray, Physica C **224**, 247 (1994).
[60] M. Capone, W. Stephan, and M. Grilli, Phys. Rev. B **56**, 4484 (1997).
[61] D. Poilblanc, Phys. Rev. B **44**, 9562 (1991).
[62] H. Fehske, G. Wellein, B. Bäuml, and R. N. Silver, Physica C **282-287**, 1829 (1997).
[63] D. B. Tanner and T. Timusk, in *Physical Properties of High-Temperature Superconductors III*, edited by D. M. Ginsberg (World Scientific, Singapore, 1992), p. 363.
[64] J. Loos and H. Fehske, Phys. Rev. B **56**, 3544 (1997).
[65] J. R. Schrieffer, X.-G. Wen, and S.-C. Zhang, Phys. Rev. Lett. **60**, 944 (1988).
[66] D. Emin, in *Polarons and Bipolarons in High-T_c Superconductors and Related Materials*, edited by E. K. H. Salje, A. S. Alexandrov, and W. Y. Liang (Cambridge University Press, Cambridge, 1995).
[67] H. G. Reik, Z. Phys. **203**, 364 (1967).
[68] Y. Y. Suzuki, P. Pincus, and A. J. Heeger, Phys. Rev. B **44**, 7127 (1991).
[69] Y. Inada and C. Ishii, J. Phys. Soc. Jpn. **59**, 612 (1990).
[70] D. Augier and D. Poilblanc, Eur. Phys. J. B **1**, 19 (1998).
[71] Q. F. Zhong, S. Sorella, and A. Parola, Phys. Rev. B **49**, 6408 (1994).
[72] E. R. Gagliano and C. A. Balseiro, Phys. Rev. Lett. **59**, 2999 (1987).
[73] R. N. Silver and H. Röder, Int. J. Mod. Phys. C **5**, 935 (1994).
[74] R. N. Silver and H. Röder, Phys. Rev. E **56**, 4822 (1997).
[75] B. Bäuml, Master's thesis, University of Bayreuth 1997 (unpublished).
[76] J. K. Cullum and R. A. Willoughby, *Lanczos Algorithms for Large Symmetric Eigenvalue Computations*, Vols. I and II (Birkhäuser, Boston, 1985).
[77] R. N. Silver, H. Röder, A. F. Voter, and J. D. Kress, Int. J. Mod. Phys. C **124**, 115 (1996).
[78] G. Wellein, B. Bäuml, and H. Fehske, in *Proceedings of the XIth International Conference on Recent Progress in Many-Body Theories, Sydney 1997*, edited by D. Neilson (World Scientific, Singapore, 1998).